Oxidation-enhanced Si self-diffusion in isotopically modulated silicon nanopillars

Cite as: J. Appl. Phys. **127**, 045704 (2020); https://doi.org/10.1063/1.5134105
Submitted: 31 October 2019 . Accepted: 10 January 2020 . Published Online: 28 January 2020

Ryotaro Kiga, Sayaka Hayashi, Satoru Miyamoto, Yasuo Shimizu, Yasuyoshi Nagai, Tetsuo Endoh, and Kohei M. Itoh

Journal of Applied Physics ARTICLE scitation.org/journal/jap

Oxidation-enhanced Si self-diffusion in isotopically modulated silicon nanopillars

Cite as: J. Appl. Phys. **127**, 045704 (2020); doi: 10.1063/1.5134105
Submitted: 31 October 2019 · Accepted: 10 January 2020 ·
Published Online: 28 January 2020

Ryotaro Kiga,[1,a)] Sayaka Hayashi,[1] Satoru Miyamoto,[1] Yasuo Shimizu,[2] Yasuyoshi Nagai,[2] Tetsuo Endoh,[3,4] and Kohei M. Itoh[1,a)]

AFFILIATIONS

[1]School of Fundamental Science and Technology, Keio University, Yokohama 223-8522, Japan
[2]Institute for Materials Research, Tohoku University, Oarai, Ibaraki 311-1313, Japan
[3]Center for Innovative Integrated Electronic Systems (CIES), Tohoku University, Sendai 980-0845, Japan
[4]JST-ACCEL, Sendai 980-0845, Japan

Note: This paper is part of the Special Topic on Defects in Semiconductors 2020.
[a)]**Authors to whom correspondence should be addressed:** kiga@keio.jp and kitoh@appi.keio.ac.jp

ABSTRACT

Silicon (Si) self-diffusivity in a Si nanopillar under dry oxidation was quantitatively evaluated by atom probe tomography of Si isotope heterostructure interfaces. Dry oxidation of a nanopillar with 200 nm diameter at 920 °C for 4 h revealed that the Si self-diffusivity was the same as the one measured for the standard planar oxidation despite the fact that the diffusion region probed in the pillar was surrounded by approximately seven times more oxidation interface areas than the simple planar oxidation case. This finding can be understood by considering the large diffusion length of ~300 μm of the interstitials for our thermal oxidation condition. The excess interstitials injected by the pillar oxidation as well as those injected by the oxidation of the base (100) plane can easily diffuse through the sample, including interiors of the pillars, making the concentration of the excess interstitials practically equal to those injected for the (100) planar oxidation case.

I. INTRODUCTION

As the conventional two-dimensional scaling of the planar metal-oxide-semiconductor field-effect transistors (MOSFETs) is approaching its limit, three-dimensional scaling is attracting much attention.[1–3] One of the possible solutions is a vertical body-channel MOSFET (vertical BC-MOSFET) in which a vertical Si nanopillar is employed as a signal channel.[4] Here, an electric gate to control the current on/off is placed on a pillar sidewall with a geometry all-around-the-pillar. Such a gate is formed by dry oxidation of the sidewall of the Si nanopillar structure followed by appropriate metallization.[5] A number of previous experiments have reported anomaly in the oxidation of Si nanopillars with respect to that of planar Si surfaces. Liu *et al.* after oxidation observed the decrease in the total number of Si atoms in the remaining Si nanopillars and oxidized layers combined and proposed (1) anomalous anisotropic diffusion of self-interstitials toward the substrate and (2) evaporation of Si from the nanopillars in the form of volatile products as possible explanations for the loss of Si atoms.[6,7] More recently, a theoretical study by Kageshima *et al.* suggested that an anomalous transport of Si atoms from the nanopillar to the substrate surface side could occur by stress induced viscous flow of surrounding SiO_2 and assigned this mechanism to be responsible for what appeared to be the loss of the total number of Si atoms after oxidation of Si nanopillars.[8] Therefore, a first obvious step toward understanding of the phenomena is to investigate the most fundamental parameter, Si self-diffusion during oxidation, within a single Si nanopillar experimentally. Recently, Si self-diffusion in Si nanopillars annealed in an *inert* ambient was studied by Südkamp *et al.* to confirm that the Si self-diffusivity was the same as that in the bulk down to a nanopillar diameter of 70 nm.[9] However, Si self-diffusion in nanopillars during oxidation has never been reported despite the above-mentioned anomalies found for oxidation of nanopillars. In this paper, we show a quantitative analysis of Si self-diffusivity in a Si nanopillar during dry oxidation and demonstrate the importance of considering interstitials injected by the oxidation of the base (100) plane and diffuse into the pillars to make the concentration of the excess interstitials equal to that under the planar (100) oxidation.

II. EXPERIMENTS

A molecular-beam-epitaxy (MBE) grown isotopically modulated Si multilayers[10] on a (100)-oriented Si wafer were lithographically made into pillars and the spatial distributions of ^{28}Si and ^{30}Si isotopes within the pillars before and after oxidation were revealed by atom probe tomography (APT). A pillar diameter of 200 nm was chosen for a reliable APT analysis before and after oxidation. Oxidation of Si nanopillars with the diameter smaller than ~70 nm would lead to the emergence of an extra parameter, oxidation-induced stress,[11–13] which would complicate our analysis. The multilayers consisted of four periods of pairs of a 25 nm-thick ^{nat}Si layer and a 50 nm-thick ^{28}Si layer, where ^{nat}Si stands for silicon with natural isotopic compositions (92.2% ^{28}Si, 4.7% ^{29}Si, and 3.1% ^{30}Si) and ^{28}Si for isotopically enriched 99.92% ^{28}Si, which were prepared by MBE. For fabrication of Si nanopillars, metal-assisted chemical etching (MACE) was employed.[14] Figure 1(a) illustrates the sequence of the sample fabrication. First, an electron beam resist (ZEON ZEP520A) was spin coated on the multilayers. Then, a two-dimensional lattice array of 200 nm diameter circles was drawn by an electron beam lithography system (Elionix, ELS-7800). After a positive resist development, deposition of 10 nm-thick Ti followed by 20 nm-thick Au films was performed on the unmasked part of the oxide-removed Si surface using a vacuum evaporator. The wafer was cut into sample pieces with lateral dimensions of 5×5 mm^2. MACE was conducted by immersing the pieces in a liquid mixture of HF (4 M) and H_2O_2 (0.4 M) for 6 min at room temperature. The resulting isotopically modulated Si nanopillar array was localized within a $\sim 1 \times 0.3$ mm^2 region of each 5×5 mm^2 sample piece. Immediately after MACE, the Au–Ti metal catalyst film on top of Si nanopillars was lift-off by solvent and the rest on the etched region was removed by aqua regia. The sample piece was then cleaned by the RCA protocol. Figure 1(b) shows a scanning electron microscope (SEM) image of an identical copy of the isotopically modulated Si nanopillar array used in the present work. SEM observation of the actual nanopillar samples was not performed because this process can lead to surface contamination that makes the pillars to be inappropriate for the surface oxidation experiment. To observe Si self-diffusion in a dry oxidation condition, the piece with the Si nanopillars was annealed in a resistance furnace at 920 °C for 4 h under the continuous flow of pure O_2 gas. In parallel, the identical sample piece with the same Si nanopillar array was annealed at the same temperature and duration in the pure argon (Ar) atmosphere for comparison.

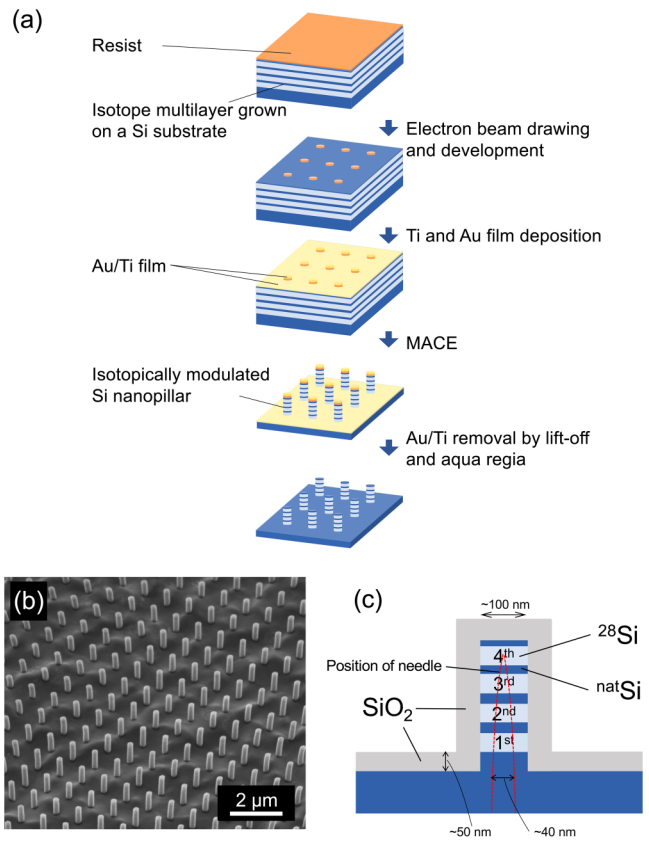

FIG. 1. (a) The fabrication procedure of the isotopically modulated Si nanopillar array. (b) A tilted scanning electron microscope image of an isotopically modulated Si nanopillar array. The diameters of the Si nanopillars are ~200 nm, and the heights are ~400 nm. (c) A schematic cross-section of an isotopically modulated Si nanopillar structure expected after surface dry oxidation. Appropriate thickness of the oxide is ~50 nm while that of the Si core diameter is ~100 nm. A red broken curve illustrates the needle-milling shape for APT.

For APT, single Si nanopillars were milled into needle specimens using a focused ion beam apparatus (Thermo Fisher Scientific, Helios NanoLab 600i). Note that the size of the needle was small enough to remove the SiO_2 layer formed on and around the pillar [Fig. 1(c)], because vertical SiO_2 leads to a nonhemispherical specimen shape during field evaporation in APT analysis and causes image distortion after data reconstruction.[15] The tip diameter was approximately 40 nm. The starting Si nanopillar diameter of 200 nm was chosen to meet these conditions.

Each 5×5 mm^2 sample piece also contained a flat, unetched ^{nat}Si/^{28}Si multilayer surface so that the reference data, oxidation-enhanced diffusion (OED) of the flat silicon (planar oxidation) under the same dry oxidation condition, were obtained from the same sample piece. The needle specimen was measured using a laser-assisted local electrode atom probe apparatus (CAMECA, LEAP4000XHR). The base temperature was stabilized at 35 K, and the pressure in the analysis chamber was approximately 3×10^{-11} Torr. The pulsed laser had a fixed wavelength of 355 nm. The repetition rate and energy were 160 or 200 kHz and 20 pJ, respectively. The detection rate of the ions was 0.008–0.012/pulse. The ratio of doubly to singly charged states, Si^{++}/Si^{+}, in the analyzed Si multilayers ranged from 174 to 282. 3D reconstructions were performed using the Integrated Visualization and Analysis Software.

III. RESULTS AND DISCUSSION

A. Determination of self-diffusion coefficients in silicon nanopillars

A reconstructed Si isotope distribution in an unannealed Si nanopillar is shown in Fig. 2(a). It shows the first three periods of isotope multilayers from the substrate in the Si nanopillar.

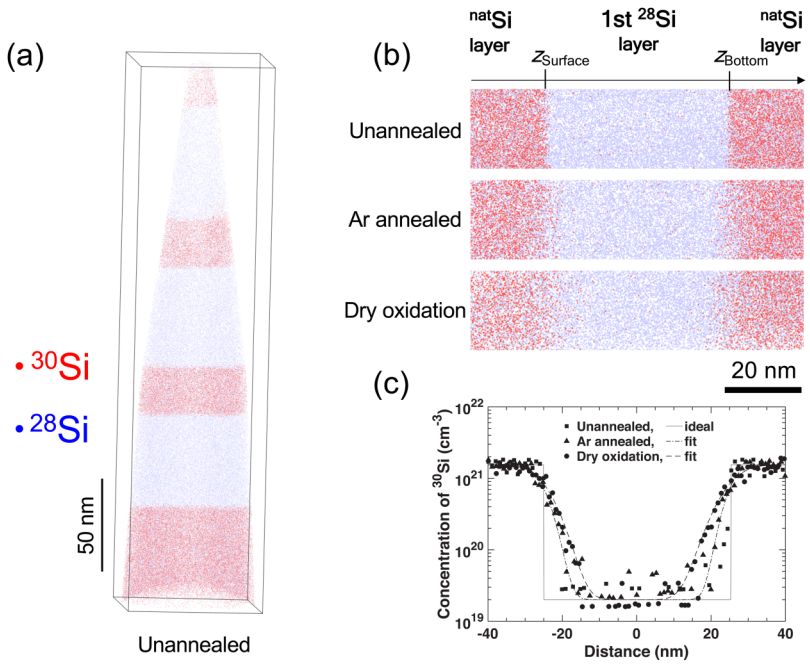

FIG. 2. (a) A 3D atom map of an unannealed isotopically modulated Si nanopillar. Red and blue dots in the atom maps represent ^{30}Si and ^{28}Si isotopes, respectively. (b) Planar projected atom maps around the first ^{28}Si enriched layers in the unannealed, Ar annealed, and dry-oxidized Si nanopillars. (c) ^{30}Si concentration profiles around the first ^{28}Si enriched layer extracted from the cylindrical regions of interest and corresponding fits by Eq. (1) for the Ar annealed and dry-oxidized Si nanopillars. The solid line represents ideal abrupt interfaces in the unannealed Si nanopillar.

In Fig. 2(b), atom maps around the first ^{28}Si layer from the substrate for the unannealed, Ar annealed, and thermally oxidized pillars are shown. As expected, isotope heterostructure interfaces in the unannealed Si nanopillar showed the most abrupt transition of the two isotopes[16,17] while the interfaces for the dry-oxidized pillar show the broadest transition. In order to determine the Si self-diffusion coefficients in the pillar, we defined a cylindrical region of interest with a diameter of 15 nm in the reconstructed atom maps. Figure 2(c) shows the 1D concentration profiles of ^{30}Si within the region of interest. Here the concentration profiles were fitted by the following equation representing the solution of Fick's law:

$$C_{\mathrm{Si}} = C_2 - \frac{C_2 - C_1}{2}\left[\mathrm{erf}\left(\frac{z - z_1}{l}\right) - \mathrm{erf}\left(\frac{z - z_2}{l}\right)\right], \qquad (1)$$

where z_1 and z_2 are the surface-side and bottom-side interfacial distances with respect to the ^{28}Si layer center, C_1 and C_2 are the minimum and maximum concentrations of ^{30}Si, respectively, and l is the diffusion length. The Si self-diffusion coefficient $D_{\mathrm{Si}}^{\mathrm{SD}}$ is then obtained by the relation $l = 2\sqrt{D_{\mathrm{Si}}^{\mathrm{SD}} t}$, where t is the duration of the thermal treatment. Experimental profiles for the three Si nanopillar samples are shown with the best fits in Fig. 2(c).

In Fig. 3, a ^{30}Si self-diffusion profile in dry-oxidized Si nanopillar is shown in comparison with that taken from the planar oxidation part of the same sample piece. Both profiles were obtained by APT. Here, excellent agreement in the concentration profiles between the nanopillar and planar part is quite clear. The diffusion lengths obtained by fitting the dry-oxidized Si nanopillar profile was $l = 7.2 \pm 1.0$ nm, while that in the planar part was $l = 7.0 \pm 1.0$ nm. These numbers agree very well within the measurement accuracy, i.e., OED in the nanopillar is the same as that in the planar sample.

In a recent experiment by Südkamp *et al.*, it was demonstrated for nanopillars of diameters less than 70 nm that the Si self-diffusion in such nanopillars are the same as those in bulk Si when annealed in an inert atmosphere, Ar gas, in the temperature ranges between 850 and 1000 °C. Such experimental results are confirmed by the present experiment as shown in Fig. 4. Here, the best fit for the ^{30}Si profile in the Si nanopillar after annealing in an Ar

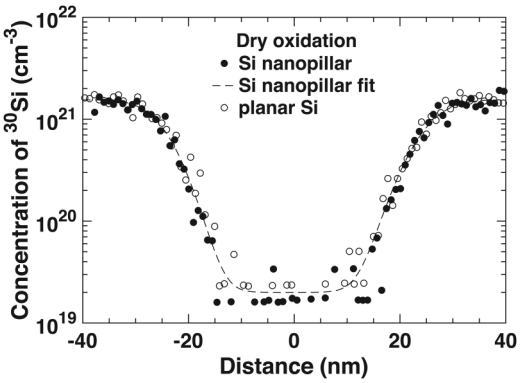

FIG. 3. Comparison of the ^{30}Si concentration profile within the first ^{28}Si enriched layer after dry oxidation between the Si nanopillar and planar area. The data points were obtained by APT. The broken line shows best fit by Eq. (1) to the dry-oxidized Si nanopillar profile.

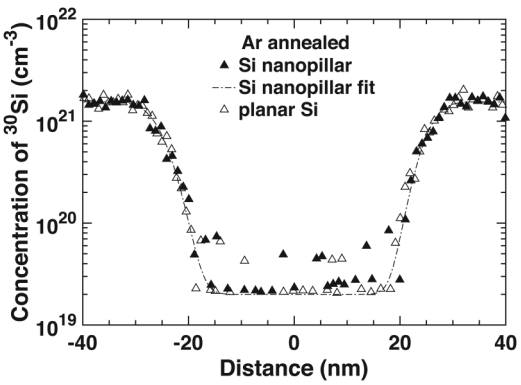

FIG. 4. Comparison of the ^{30}Si concentration profile within the first ^{28}Si enriched layer after inert (Ar) annealing between the Si nanopillar and planar area. The data points were obtained by APT. The dashed line shows the best fit by Eq. (1) to the profile of ^{30}Si in the Si nanopillar.

atmosphere shows the Si self-diffusion length $l = 4.6 \pm 1.0$ nm, which is comparable with that of the bulk $l = 4.9 \pm 1.0$ nm.

B. Secondary ion mass spectrometry (SIMS) verification of the diffusivity obtained by APT

In order to confirm the validity of the diffusivity obtained by our APT analysis, a set of planar experiments were performed by secondary ion mass spectrometry (SIMS) for comparison. Figure 5 shows the representing results. The SIMS profiles after the thermal treatments were analyzed using a numerical solver, assuming unannealed SIMS data as the initial profile. The planar dry-oxidized sample shows a diffusion length of $l = 7.4 \pm 0.4$ nm. Here, good agreement between the diffusion lengths obtained by SIMS and APT for the planar dry-oxidized sample confirms the overall reliability of our measurements and analysis. Indeed, the planar

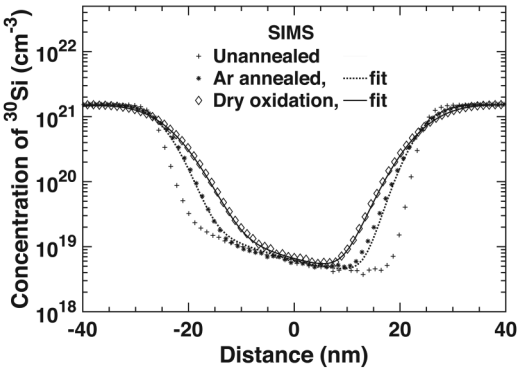

FIG. 5. ^{30}Si concentration profiles analyzed by SIMS in the planar experiments. Cross, asterisk, and diamond symbols represent the results of unannealed, Ar annealed, and dry-oxidized samples, respectively. The lines represent the best fits for experimental profiles calculated by a numerical solver.

TABLE I. Si self-diffusion coefficients D_{Si}^{SD} determined in Si nanopillars with a diameter of 200 nm for both Ar annealing and dry oxidation at 920 °C for 4 h. Values of planar experiments determined by SIMS and APT are also listed.

	$D_{Si}^{SD}(\times 10^{-18}$ cm^2 s$^{-1})$	
	SIMS	APT
Ar annealed planar Si	4.2 ± 0.8	4.2 ± 2.0
Ar annealed Si nanopillar	…	3.7 ± 2.0
Dry-oxidized planar Si	9.5 ± 1.1	8.5 ± 2.6
Dry-oxidized Si nanopillar	…	9.0 ± 2.7

sample annealed in the inert atmosphere showed a diffusion length of $l = 4.9 \pm 0.4$ nm for our annealing condition, and it agrees with results reported in the literature for the intrinsic Si self-diffusion experiments.[18–20] The increase in Si self-diffusion observed in dry oxidation represents the oxidation-enhanced diffusion (OED). The ~2.3 times enhancement of Si self-diffusivity obtained here is also in good agreement with the value from the literature.[21]

Si self-diffusion coefficients obtained in the present work together with the diffusion coefficients measured by SIMS are summarized in Table I.

C. Interpretation

We shall now explain why the OEDs of Si self-diffusion are the same for the nanopillar and flat surface. When viewed from the middle [point A in Fig. 6(a)] of the nanopillar employed in this study, the surface area, i.e., the Si/SiO$_2$ interface area, is approximately seven times larger than the view from 100 nm below the flat Si wafer [point B in Fig. 6(a)]. Therefore, one may argue that there is approximately seven times increase in the interstitial silicon concentration (C_I) in the nanopillar to further enhance the Si self-diffusion. However, our experimental results suggest that C_I in the pillar does not exceed that in the planar oxidation of (100)-oriented silicon and, therefore, OED of Si self-diffusion remains the same even in the pillar. During thermal oxidation of Si, oxygen atoms in the atmosphere enter SiO$_2$ and diffuse through the oxide to reach the Si/SiO$_2$ interface at which further oxidation takes place.[22] The rate of oxidation is well known for the oxidation of the planar Si surface for a given combination of orientations, annealing temperature, O$_2$ partial pressure, and oxide thickness.[23,24] Also, it is well known that the interfacial reaction produces a fixed amount of excess Si atoms per unit interfacial area for a given oxidation condition at the Si/SiO$_2$ interface.[25,26] As schematically shown in Fig. 6(b), the excess Si atoms produced at the Si/SiO$_2$ interface ($d = 0$) divide themselves to behave in the following three ways: (I) outward emission toward the SiO$_2$ film, (II) recombination to the Si crystal at the Si/SiO$_2$ interface, and (III) inward diffusion into the Si crystal as self-interstitials.[27,28] Here, the concentration of self-interstitials injected into the Si crystal (C_I) is determined by the concentration-gradient of C_I in the Si side of the Si/SiO$_2$ interface. As the oxidation proceeds, because of the extremely long diffusion length of interstitials,[29] ~300 μm for our 920 °C for 4 h condition, C_I in the Si crystal practically reaches the concentration of the

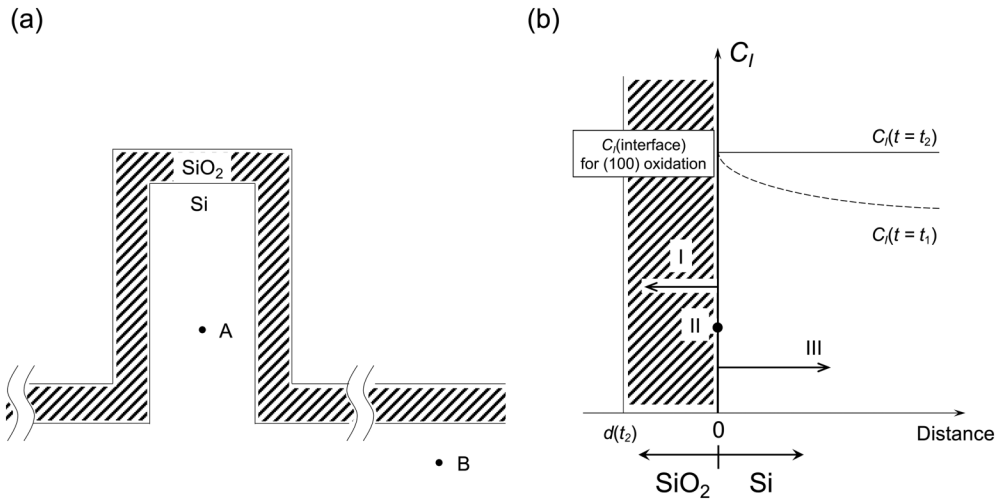

FIG. 6. (a) A schematic of Si nanopillar top and sidewall oxidation showing approximately seven times more oxidation interface area surrounding point A in the Si nanopillar with respect to point B under the flat oxidation area. (b) Three migration paths of excess Si produced at the SiO_2/Si interfaces during dry oxidation: (I) outwards emission toward the SiO_2 film, (II) recombination to the Si crystal at the Si/SiO_2 interface, and (III) inward diffusion into the Si crystal as self-interstitials. The origin of the horizontal axis is taken at the interface of SiO_2 and Si, with the positive (negative) side being silicon (SiO_2). Broken and solid curves on the right top show representing examples of Si interstitials profiles $C_I(t = t_1)$ and $C_I(t = t_2)$, for dry oxidation durations of $t = t_1$ and t_2, respectively, where t_1 is just after the beginning of the oxidation and t_2 shows C_I after saturation. $d(t_2)$ shows the outer surface positions of the growing SiO_2 film for t_2.

excess Si at the interface [C_I (interface) at $d = 0$] in Fig. 6(b), so the gradient of C_I in the Si side diminishes.[30] The amount of excess interstitials injected into the bulk during thermal oxidation depends on the orientation of the oxidation surface, (100) being the largest while (110) being less.[31] Because our pillars are formed on the (100) plane, the cylindrical sidewall of the pillar has a four-fold symmetry consisting of continuous combinations of (100) and (110) planes. Therefore, in the case of oxidation of the sidewall surface of the pillar, the largest injection of excess interstitials occurs at the four (100) sidewalls and those excess interstitials can laterally diffuse to the adjacent (110) sidewalls. Such interstitials can be absorbed at the (110) sidewall oxidation interface, i.e., simulations assuming an appropriate range of the (110) sidewall absorption of interstitials are needed to precisely model the thermal oxidation behavior of the nanopillar sidewalls.

However, the present experimental finding of OED in the pillar being the same as those of the (100) planar oxidation made us realize one very important path to sustain the high level of excess interstitials in the pillars. It is well established that the diffusivity of Si interstitials at 920 °C is $D_I = 1.7 \times 10^{-6}$ cm^2 s^{-1} and the corresponding diffusion length for the 4 h annealing is $\sim 300\,\mu$m.[29] This fact prompts us to consider another larger excess Si interstitial injection place: the oxide/silicon interface of the (100) base plane on which pillars are standing. In our sample geometry, the ratio of surface areas of the pillar sidewalls to the (100) base plane is $\sim 1{:}10^5$. Therefore, the large amount of excess Si interstitials injected during the oxidation of the (100) base plane diffuses into all pillars and makes the excess concentration of interstitials in the pillars same as that at the (100) oxide/silicon interface during oxidation. Of course, many interstitials diffused into the pillars are absorbed at the (110) sidewall interfaces, but the amount coming from the bulk overwhelms to make the concentration of the excess interstitials practically constant. Such an argument makes it clear that the saturated C_I level at point A in Fig. 6(a) and the nearly saturated C_I level at point B are practically the same. Because Si self-diffusivity under oxidation is governed by the amount of the excess Si interstitial concentration, the experimental observation of oxidation-enhanced Si self-diffusivity in the nanopillar turns out to be the same. Therefore, our surface dry oxidation experiment for the Si nanopillar with 200 nm diameter at 920 °C for 4 h has shown that the OED model established for planar oxidation can be applied to the Si nanopillar sidewall and top oxidation.

It should be noted that the present results enhance the mystery of previously reported nanopillar oxidation anomaly: observation of the decrease in the total number of Si atoms in the remaining Si nanopillars and oxidized layers combined.[6,7] Those experiments were performed also on the pillars standing on the (100) base planes and the oxidation was taking place not only on the pillar surfaces but also on the (100) base planes. Therefore, it is natural to assume that the excess interstitials were flowing into the pillars from the bulk. Yet they reported the loss of silicon atoms from the pillars after oxidation. Further investigations are clearly needed to solve such a mystery.

IV. CONCLUSIONS

We have quantitatively evaluated self-diffusion in isotopically modulated Si nanopillars with a diameter of 200 nm for both dry oxidation and Ar annealed conditions using atom probe tomography. In the Ar annealed experiment, self-diffusivity in the Si

nanopillar was found to be the same as the one measured in bulk Si and it confirmed the finding reported by Südkamp *et al.*[9] In the dry oxidation experiment, oxidation-enhanced Si self-diffusivities in the nanopillar were also found to be the same as those obtained with the planar part of the same Si samples, showing that the planar oxidation-enhanced diffusion model is applicable in the Si nanopillar of the present experiment, where the excess interstitial injection occurs also from the bulk side as a result of the oxidation of the base (100) plane on which the nanopillars are standing.

ACKNOWLEDGMENTS

We acknowledge Masashi Uematsu for fruitful discussions and Keiko Tomura and Naoki Ebisawa for technical support. This work was supported by a grant from "Three-Dimensional Integrated Circuits Technology Based on Vertical BC-MOSFET and Its Advanced Application Exploration" of ACCEL under the Japan Science and Technology Agency (Research Director: Professor Tetsuo Endoh; Program Manager: Dr. Toru Masaoka) of ACCEL under JST (JPMJAC1301), JSPS KAKENHI (Grant No. 15H05413), and by the Center for Spintronics Research Network at Keio University.

REFERENCES

[1]D. J. Frank, R. H. Dennard, E. Nowak, P. M. Solomon, Y. Taur, and H. P. Wong, Proc. IEEE **89**, 259 (2001).
[2]T. Endoh, K. Kinoshita, T. Tanigami, Y. Wada, K. Sato, K. Yamada, T. Yokoyama, N. Takeuchi, K. Tanaka, N. Awaya, K. Sakiyama, and F. Masuoka, IEEE Trans. Electron Devices **50**, 945 (2003).
[3]A. Veloso, B. Parvais, P. Matagne, E. Simoen, T. Huynh-Bao, V. Paraschiv, E. Vecchio, K. Devriendt, E. Rosseel, E. Ercken, B. T. Chan, C. Delvaux, E. Altamirano-Sánchez, J. J. Versluijs, Z. Tao, S. Suhard, S. Brus, A. Sibaja-Hernandez, N. Waldron, P. Lagrain, O. Richard, H. Bender, A. Chasin, B. Kaczer, T. Ivanov, S. Ramesh, K. De Meyer, J. Ryckaert, N. Collaert, and A. Thean, in *2016 IEEE Symposium on VLSI Technology, Honolulu, HI, 14–16 June 2016* (IEEE, 2016).
[4]T. Endoh, K. Sakui, and Y. Yasuda, IEICE Trans. Electron. **E93-C**, 557 (2010).
[5]B. Yang, K. D. Buddharaju, S. H. G. Teo, N. Singh, G. Q. Lo, and D. L. Kwong, IEEE Electron Device Lett. **29**, 791 (2008).
[6]H. I. Liu, N. I. Maluf, R. F. W. Pease, D. K. Biegelsen, N. M. Johnson, and F. A. Ponce, J. Vac. Sci. Technol. B **10**, 2846 (1992).
[7]H. I. Liu, D. K. Biegelsen, N. M. Johnson, F. A. Ponce, and R. F. W. Pease, J. Vac. Sci. Technol. B **11**, 2532 (1993).
[8]H. Kageshima, K. Shiraishi, and T. Endoh, Jpn. J. Appl. Phys. **57**, 06KD02 (2018).
[9]T. Südkamp, G. Hamdana, M. Descoins, D. Mangelinck, H. S. Wasisto, E. Peiner, and H. Bracht, J. Appl. Phys. **123**, 161515 (2018).
[10]T. Kojima, R. Nebashi, K. M. Itoh, and Y. Shiraki, Appl. Phys. Lett. **83**, 2318 (2003).
[11]D. B. Kao, J. P. McVittie, W. D. Nix, and K. C. Saraswat, IEEE Trans. Electron Devices **34**, 1008 (1987).
[12]D.-B. Kao, J. P. McVittie, W. D. Nix, and K. C. Saraswat, IEEE Trans. Electron Devices **35**, 25 (1988).
[13]C. C. Büttner and M. Zacharias, Appl. Phys. Lett. **89**, 263106 (2006).
[14]K. Yamada, M. Yamada, H. Maki, and K. M. Itoh, Nanotechnology **29**, 28LT01 (2018).
[15]D. Melkonyan, C. Fleischmann, L. Arnoldi, J. Demeulemeester, A. Kumar, J. Bogdanowicz, F. Vurpillot, and W. Vandervorst, Ultramicroscopy **179**, 100 (2017).
[16]Y. Shimizu, Y. Kawamura, M. Uematsu, K. M. Itoh, M. Tomita, M. Sasaki, H. Uchida, and M. Takahashi, J. Appl. Phys. **106**, 076102 (2009).
[17]Y. Shimizu, Y. Kawamura, M. Uematsu, M. Tomita, T. Kinno, N. Okada, M. Kato, H. Uchida, M. Takahashi, H. Ito, H. Ishikawa, Y. Ohji, H. Takamizawa, Y. Nagai, and K. M. Itoh, J. Appl. Phys. **109**, 036102 (2011).
[18]H. Bracht, H. H. Silvestri, I. D. Sharp, and E. E. Haller, Phys. Rev. B **75**, 035211 (2007).
[19]Y. Shimizu, M. Uematsu, and K. M. Itoh, Phys. Rev. Lett. **98**, 095901 (2007).
[20]T. Südkamp and H. Bracht, Phys. Rev. B **94**, 125208 (2016).
[21]A. Ural, P. B. Griffin, and J. D. Plummer, Phys. Rev. Lett. **83**, 3454 (1999).
[22]J. R. Ligenza and W. G. Spitzer, J. Phys. Chem. Solids **14**, 131 (1960).
[23]B. E. Deal and A. S. Grove, J. Appl. Phys. **36**, 3770 (1965).
[24]H. Z. Massoud, J. D. Plummer, and E. A. Irene, J. Electrochem. Soc. **132**, 1745 (1985).
[25]S. T. Dunham and J. D. Plummer, J. Appl. Phys. **59**, 2541 (1986).
[26]S. T. Dunham and J. D. Plummer, J. Appl. Phys. **59**, 2551 (1986).
[27]S. T. Dunham, J. Electrochem. Soc. **136**, 250 (1989).
[28]S. Fukatsu, T. Takahashi, K. M. Itoh, M. Uematsu, A. Fujiwara, H. Kageshima, Y. Takahashi, K. Shiraishi, and U. Gösele, Appl. Phys. Lett. **83**, 3897 (2003).
[29]H. Bracht, N. A. Stolwijk, and H. Mehrer, Phys. Rev. B **52**, 16542 (1995).
[30]A. M. Agarwal and S. T. Dunham, Appl. Phys. Lett. **63**, 800 (1993).
[31]P. M. Fahey, P. B. Griffin, and J. D. Plummer, Rev. Mod. Phys. **61**, 289 (1989).